Journal of Thermal Analysis and Calorimetry (2021) 144:1389–1399
https://doi.org/10.1007/s10973-020-09664-1

Heat transfer of viscous fluid in a vertical channel sandwiched between nanofluid porous zones

Jawali C. Umavathi[1] · **Mikhail A. Sheremet**[2]

Received: 10 November 2019 / Accepted: 3 April 2020 / Published online: 15 April 2020

Abstract

Mixed convection in vertical parallel channels is analyzed with the viscous fluid sandwiched between nanofluids within porous material filled in a vertical channel. The concept of single-phase transport of nanofluids is employed to define the nanofluid flow and heat transfer and the Darcy approach is incorporated to describe the circulation within the porous material. Formulated ordinary differential equations which are non-linear and coupled along with the corresponding boundary and interface conditions are solved by the regular perturbation method. The main objective is to investigate the effects of the Grashof and Brinkman numbers, solid volume fraction, porous parameter on the velocity and temperature fields. Results are shown in the graphical and tabular form. The physical characteristics governing the flow such as skin friction and rate of heat transfer are also investigated considering five different materials of nanoparticles.

Keywords Mixed convection · Nanofluid · Darcy model · Vertical channel · Perturbation method

Abbreviations

Br Brinkman number $\left(Br = \frac{\mu_f^3}{\rho_f^2 h^2 (T_{w1} - T_{w2}) k_f}\right)$
G Acceleration due to gravity
Gr Grashof number $\left(Gr = \frac{g\beta_f (T_{w1} - T_{w2})\, h^3}{\upsilon_f^2}\right)$
h Channel width
k Thermal conductivity
P Non-dimensional pressure $\left(P = -\frac{\rho_f h^3}{\mu_f^2} \frac{\partial p}{\partial x}\right)$
T Temperature
u Dimensional velocity
y Space coordinate

Greek symbols

β Thermal expansion coefficient
θ Dimensionless temperature
μ Dynamic viscosity
ν Kinematic viscosity
ρ Density
σ Porous parameter $\left(\sigma = h \Big/ \sqrt{\kappa}\right)$
τ Skin friction
ϕ Volume fraction of the solid nanoparticles

Subscripts

nf Nanofluid
f Base fluid
s Solid nanoparticles
i Quantities for the fluids in region-I, region-II and region-III

Introduction

In a wide range of industrial applications, low performance of convective heat transfer rate for cooling systems is intensified. Heat transfer fluid has drawn the attention to augment the energy transport intensity for a period of more than five decades. Dispersing millimeter- and micrometer-sized particles from the material of high thermal conductivity was opted initially to enhance the energy transport of thermal fluids. A theoretical formula was predicted by Maxwell [1] for the evaluation of thermal conductivity of suspensions. But millimeter or micrometer-sized particles did not find true applications in industry owing to rapid settling, high pressure drop, clogging small channels, erosion and low energy transport intensity at low concentrations.

A new class of heat transfer fluids known as nanofluids comprises of liquid suspensions of nanometer-sized

✉ Mikhail A. Sheremet
Michael-sher@yandex.ru

[1] Department of Mathematics, Gulbarga University, Kalaburgi, Karnataka 585106, India

[2] Regional Scientific and Educational Mathematical Centre, Tomsk State University, Tomsk, Russia 634050

particles. Many researchers in the community investigated the merits of dispersing nanometer-sized particles into base fluids to enhance heat transfer in mixed convection settings [2–5]. Thus, Abu-Nada and Chamkha [6] conducted a computational study on mixed convection in a lid-driven cavity filled with nanofluids ($H_2O + Al_2O_3$). Significant heat transfer enhancement was observed in the study due to the addition of nanoparticles. Tiwari and Das [7] studied heat transfer augmentation in two-sided nanofluid filled in a lid-driven cavity. They solved two-dimensional single-phase equations using the finite volume method and observed the need for high Richardson number to move nanofluid at higher solid volume fraction as a result of the increased viscosity of nanofluid compared to the base fluids. A study of using different nanofluids on lid-driven porous cavities in mixed convections was performed by Mittal et al. [8]. Bianco et al. [9] published a book on heat transfer enhancement with nanofluid. Modeling convection in nanofluids from clear fluid to porous media for both natural and forced convection was narrated in Chapter 11 of Bianco et al. [9] by Nield and Kuznetsov. The size of nanoparticles varies from 1 to 100 nm suspended in base fluids such water [10, 11], ethylene glycol [12], methanol [13] and engine oil [14] constitutes for different types of nanofluids. Compared to traditional heat transfer fluids, the metallic or non-metallic suspended particles have higher thermal conductivities. Hence the transport and thermal properties of base fluids are significantly changed by the suspended nanoparticles. A noticeable increase of heat transfer was investigated using copper as nanoparticles [15–18], copper oxide as nanoparticles [19, 20] and carbon nanotubes [21] and keeping water as base fluid. Bianco et al. [22] analyzed turbulent forced convection flow of water-Al_2O_3 nanofluid in a circular tube. They concluded that convective heat transfer for nanofluid was greater than that of the base fluid. Sheikholeslami et al. [23] employing CVFEM designed alumina nanofluid magneto hydrodynamic flow through permeable enclosure. He warped up that Lorentz forces boost the conduction mechanism, whereas average Nusselt number declines with strengthening of Hartmann number. The boundary layer was pruned augmenting the radiation parameter. Lorentz forces impact on nanoenhanced PCM (phase change material) heat transfer during discharging process was simulated by Sheikholeslami et al. [24] in a storage porous unit. He revealed that employing Lorentz forces can augment the discharging rate. Further discharging time was decreased by the presence of nanoparticles.

More than a century heat transfer in porous media was studied. Heat transfer in porous media with nanofluid under the convective mode was also taken into investigation [25]. The double-diffusive convective heat transfer past a vertical plate using nanofluids was revisited by Nield and Kuznetsov [26] employing the analytic solutions of Cheng and Minkowycz's problem [27]. The Brownian diffusion and thermophoresis effects were also taken into account. The linear and non-linear stability investigation for the onset of convection in a horizontal part of porous material with nanoliquid was examined by Umavathi and Mohite [28]. The observations on the stationary and oscillatory convection for the effects of controlling parameters were also focused in the analysis. Steady mixed convection boundary layer circulation past a vertical plate placed in a porous material with nanofluids was studied numerically by Ahmed and Pop [29]. The nanoparticles such as Al_2O_3, Cu and TiO_2 using water as a base fluid were employed to study the effects of mixed convection parameter and volume fraction. Sheikholeslami [30] modeled magnetic field influence on CuO–H_2O nanofluid convective flow in a permeable cavity considering various shapes of nanoparticles. The conclusions extracted were that selecting the platelet shape of nanoparticles the peak values of heat transfer rate was obtained in accordance with other shapes of nanoparticles. Nusselt number was accelerated with Darcy and Reynolds number, while it was shrunk with Lorentz forces.

Steady fully developed mixed convective flow using copper, alumina and titanium oxide as nanoparticles and water as a base fluid was also studied numerically by Cimpean and Pop [31]. They concluded that by adding even small amount of nanoparticles resulted with greater enhancement in the heat transfer. Mixed convective heat transfer of nanofluid in a vertical channel partially saturated by a porous medium was analyzed by Hajipour and Dehkordi [32]. The result drawn was that the Nusselt number at the cold wall was raised by an increment of the nanoparticle mass flux. Further they also concluded that increasing buoyancy force and viscous dissipation leads to the enhancement of velocity and temperature. Using CFD technique, Amrei and Dehkordi [33] studied the mixed convection in a vertical porous and regular channel for clear and nanofluid. Some interesting results on nanofluid flow in vertical channels can be found in [34–36]. Recently Sheikholeslami [37] inspected Al_2O_3-water nanofluid saturated within porous medium for the conducting fluid. He opted a new method which is Control Volume Finite Element Method (CVFEM) to solve the balance equations due to complex shape of porous cavity. He proved that the convection detracts with augmentation of magnetic forces and radiation abates the temperature gradient.

Taking into account the nanofluids applications, the objective of this work is to understand heat transfer of the viscous fluid sandwiched between two nanofluid zones saturated within the porous medium. There is no much work found in the literature for the study of immiscible nanofluids. Hence this work will focus on the heat transfer performance in a vertical channel with three areas filled with different fluids, namely central part is filled with viscous fluid, while two peripheral zones are filled with

nanofluid saturated within the porous medium. Further the important assumptions made is that the velocities, shear stresses, temperatures and heat flux are equal at the two interfaces as proposed by Vafai and Thiyagaraja [38].

Mathematical formulation

A schematic representation of the geometry along with boundary conditions is presented in Fig. 1. The channel is filled with three immiscible fluids. The fluids are assumed to be Newtonian, incompressible and the motion is steady, laminar and fully developed. The nanoliquid within porous material occupies the regions $-h \le Y \le 0$ and $h \le Y \le 2\ h$ having viscosity μ_{nf}, density ρ_{nf}, thermal expansion coefficient β_{nf}, thermal conductivity k_{nf} and permeability κ. The region $0 \le Y \le h$ is filled with Newtonian fluid having viscosity μ_f, density ρ_f, thermal expansion coefficient β_f and the thermal conductivity k_f. The Boussinesq approximation (density in the buoyancy term is variable) is incorporated along with constant thermo-physical properties. The flow in the channel is caused by the buoyancy forces. The temperature of the left wall T_{w1} is higher than that of the right wall T_{w2}. Following Vafai and Thiyagaraja [38], the velocities, shear stresses, temperatures and heat flux are assumed to be equal at the two interfaces and are implemented in the analysis.

The governing equations of heat transfer and fluid flow for nanofluid (Region-I and III) adopting Tiwari and Das model [7] and for regular fluid (Region-II) can be obtained as follows:

Region-I [7, 38]

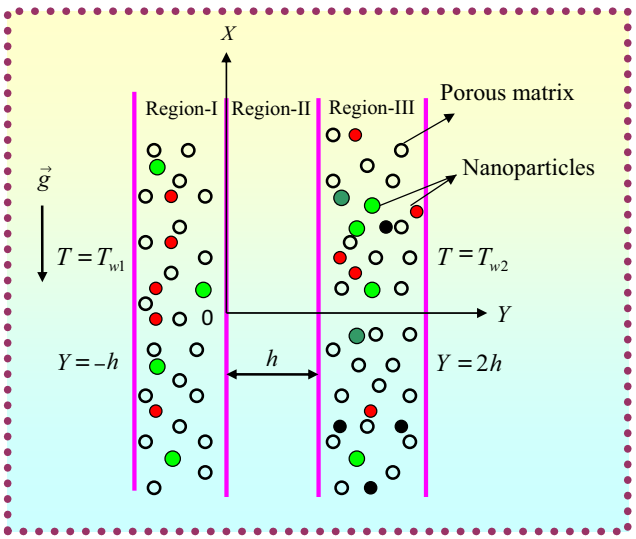

Fig. 1 Physical configuration

$$\frac{d^2u_1}{dY^2} - \frac{1}{\kappa}u_1 = -\frac{g(\rho\beta)_{nf}}{\mu_{nf}}\left(T_1 - T_{w2}\right) + \frac{1}{\mu_{nf}}\frac{\partial p}{\partial X} \tag{1}$$

$$\frac{d^2T_1}{dY^2} = -\frac{\mu_{nf}}{k_{nf}}\left(\frac{1}{\kappa}\,u_1^2 + \left(\frac{du_1}{dY}\right)^2\right) \tag{2}$$

Region-II [38]

$$\frac{d^2u_2}{dY^2} = -\frac{g\,(\rho\beta)_f}{\mu_f}\left(T_2 - T_{w2}\right) + \frac{1}{\mu_f}\frac{\partial p}{\partial X} \tag{3}$$

$$\frac{d^2T_2}{dY^2} = -\frac{\mu_f}{k_f}\left(\frac{du_2}{dY}\right)^2 \tag{4}$$

Region-III [7, 38]

$$\frac{d^2u_3}{dY^2} - \frac{1}{\kappa}u_3 = \frac{g(\rho\beta)_{nf}}{\mu_{nf}}\left(T_3 - T_{w2}\right) + \frac{1}{\mu_{nf}}\frac{\partial p}{\partial X} \tag{5}$$

$$\frac{d^2T_3}{dY^2} = -\frac{\mu_{nf}}{k_{nf}}\left(\frac{1}{\kappa}u_3^2 + \left(\frac{du_3}{dY}\right)^2\right) \tag{6}$$

Integrating the Eqs. (1), (3) and (5), one obtains six integrating constants which need to be defined using boundary and interface conditions. Two conditions at the external borders $Y=-h$ and $Y = 2h\left(u_1(-h) = 0,\ u_3(2h) = 0\right)$ which are no slip conditions and four conditions at the two interfaces $Y=0$ and $Y = h$ $\left\{\begin{array}{l} u_1(0) = u_2(0) \\ \mu_{nf}\dfrac{du_1\,(0)}{dY} = \mu_f\dfrac{du_2(0)}{dY} \end{array}\right.$ $\left\{\begin{array}{l} u_2(h) = u_3(h) \\ \mu_f\dfrac{du_2\,(h)}{dY} = \mu_{nf}\dfrac{du_3(h)}{dY} \end{array}\right)$ such as continuity of velocity and shear stress are employed to solve the six integrating constants. The integrating constants obtained from Eqs. (2), (4) and (6) are evaluated using constant wall temperatures at the external boundaries $Y = -h$ and $Y = 2\ h$ $\left(T_1(-h) = T_{w1},\quad T_3(2h) = T_{w2}\right)$ and four conditions at the interfaces $Y=0$ and $Y = h$ $\left\{\begin{array}{c} T_1(0) = T_2(0) \\ k_{nf}\dfrac{dT_1(0)}{dY} = k_f\dfrac{dT_2(0)}{dY} \end{array}\right.$ $\left\{\begin{array}{c} T_2(h) = T_3(h) \\ k_f\dfrac{dT_2(h)}{dY} = k_{nf}\dfrac{dT_3(h)}{dY} \end{array}\right)$ which are continuity of temperature and heat flux. In view of this, the boundary and interface conditions for the velocity and temperature results are as follows:

$$\begin{array}{l} u_1(-h) = 0, \quad u_1(0) = u_2(0), \quad \mu_{nf}\dfrac{du_1\,(0)}{dY} = \mu_f\dfrac{du_2(0)}{dY} \\ u_2(h) = u_3(h), \quad \mu_f\dfrac{du_2\,(h)}{dY} = \mu_{nf}\dfrac{du_3(h)}{dY}, \quad u_3(2h) = 0 \end{array} \tag{7}$$

$$T_1(-h) = T_{w1}, \quad T_1(0) = T_2(0), \quad k_{nf}\frac{dT_1(0)}{dY} = k_f\frac{dT_2(0)}{dY},$$
$$T_2(h) = T_3(h), \quad k_f\frac{dT_2(h)}{dY} = k_{nf}\frac{dT_3(h)}{dY} \quad T_3(2h) = T_{w2} \tag{8}$$

The heat capacitance, thermal expansion coefficients, thermal diffusivity and density relations for the nanofluid are considered as

$$\left(\rho C_p\right)_{nf} = (1-\phi)\left(\rho C_p\right)_f + \phi\left(\rho C_p\right)_s \tag{9}$$

$$(\rho\beta)_{nf} = (1-\phi)(\rho\beta)_f + \phi(\rho\beta)_s \tag{10}$$

$$\alpha_{nf} = \frac{k_{nf}}{\left(\rho C_p\right)_{nf}} \tag{11}$$

$$\rho_{nf} = (1-\phi)\rho_f + \phi\rho_s \tag{12}$$

Following Brinkman [39], the nanofluid viscosity is taken as

$$\mu_{nf} = \frac{\mu_f}{(1-\phi)^{2.5}} \tag{13}$$

Maxwell [1] defined the thermal conductivity for the spherical nanoparticles as

$$k_{nf} = k_f\left(\frac{2k_f - 2\phi\left(k_f - k_s\right) + k_s}{2k_f + \phi\left(k_f - k_s\right) + k_s}\right) \tag{14}$$

Table 1 documents the values of physical parameters for pure water and different nanoparticles. Further the following transformations are implemented to transform Eqs. (1)–(8) in the dimensionless format.

$$y = \frac{Y}{h}, \quad u_1^* = u_i\left(\frac{\rho_f}{\mu_f}\right)h, \quad \theta_i = \frac{T_i - T_{w2}}{T_{w1} - T_{w2}},$$
$$\sigma = \frac{h}{\sqrt{\kappa}}, \quad P = -\frac{\rho_f h^3}{\mu_f^2}\frac{\partial p}{\partial X}, Gr = \frac{g\beta_f\left(T_{w1} - T_{w2}\right)h^3}{\upsilon_f^2}, \tag{15}$$
$$Br = \frac{\mu_f^3}{\rho_f^2 h^2\left(T_{w1} - T_{w2}\right)k_f}$$

The dimensionless format of Eqs. (1)–(8) after dropping asterisks becomes

Region-I

$$\frac{d^2u_1}{dy^2} - \sigma^2 u_1 = -\left((1-\phi) + \frac{\phi(\rho\beta)_s}{(\rho\beta)_f}\right)(1-\phi)^{2.5} Gr\,\theta_1 - (1-\phi)^{2.5}\quad P \tag{16}$$

$$\frac{d^2\theta_1}{dy^2} = -\left(\frac{2k_f + \phi(k_f - k_s) + k_s}{2k_f - 2\phi(k_f - k_s) + k_s}\right) \frac{1}{(1-\phi)^{2.5}}\left(\sigma^2\quad Br\,u_1^2 + Br\left(\frac{du_1}{dy}\right)^2\right) \tag{17}$$

Region-II

$$\frac{d^2u_2}{dy^2} = -Gr\,\theta_2 - P \tag{18}$$

$$\frac{d^2\theta_2}{dy^2} = -Br\left(\frac{du_2}{dy}\right)^2 \tag{19}$$

Region-III

$$\frac{d^2u_3}{dy^2} - \sigma^2 u_3 = -(1-\phi)^{2.5}\left((1-\phi) + \frac{\phi(\rho\beta)_s}{(\rho\beta)_f}\right) Gr\,\theta_3 - (1-\phi)^{2.5}P \tag{20}$$

$$\frac{d^2\theta_3}{dy^2} = -\frac{1}{(1-\phi)^{2.5}}\left(\frac{2k_f + \phi(k_f - k_s) + k_s}{2k_f - 2\phi(k_f - k_s) + k_s}\right) \left(Br\,\sigma^2 u_3^2 + Br\left(\frac{du_3}{dy}\right)^2\right) \tag{21}$$

The boundary and interface conditions in the dimensionless form are

$$u_1(-1) = 0, \quad u_1(0) = u_2(0), \quad \frac{du_1(0)}{dy} = \frac{\mu_f}{\mu_{nf}}\frac{du_2(0)}{dy},$$
$$u_2(1) = u_3(1), \quad \frac{du_2(1)}{dy} = \frac{\mu_{nf}}{\mu_f}\frac{du_3(1)}{dy}, \quad u_3(2) = 0 \tag{22}$$

Table 1 Values of physical properties

Property	Pure water	Ag	Cu	Diamond	SiO_2	TiO_2
ρ/kg m^{-3}	997.10	10,500	8933	3510	2200	4250
μ/Pa s	0.001	–	–	–	–	–
k/W m^{-1}K^{-1}	0.613	429	400	1000	1.2	8.5938
C_p/J kg^{-1} K^{-1}	4179	235	385	497.26	703	686.2
β/K^{-1}	207×10^{-6}	18×10^{-6}	17×10^{-6}	10^{-6}	5.5×10^{-6}	0.17×10^{-6}

$$\theta_1(-1)=0,\quad \theta_1(0)=\theta_2(0),\quad \frac{d\theta_1(0)}{\mathrm{d}y}=\frac{k_\mathrm{f}}{k_\mathrm{nf}}\frac{d\theta_2(0)}{\mathrm{d}y}$$
$$\theta_2(1)=\theta_3(1),\ \frac{d\theta_2(1)}{\mathrm{d}y}=\frac{k_\mathrm{nf}}{k_\mathrm{f}}\frac{d\theta_3(1)}{\mathrm{d}y},\quad \theta_3(2)=1 \tag{23}$$

Method of solution

Exact analytical solutions cannot be found for Eqs. (16)–(21) as they are coupled and non-linear ordinary equations. Therefore approximate analytical solutions are defined by the regular perturbation technique. The Brinkman number is employed as the perturbation characteristic and this choice is justified as in many of the applications its value cannot exceed the value one. Hence the approximate solutions for the flow field can be put in the perturbation series solution as

$$u_\mathrm{i}(y)=u_{\mathrm{i}0}(y)+Br\,u_{\mathrm{i}1}(y)+Br^2\,u_{\mathrm{i}2}(y)+\cdots \tag{24}$$

$$\theta_\mathrm{i}(y)=\theta_{\mathrm{i}0}(y)+Br\,\theta_{\mathrm{i}1}(y)+Br^2\,\theta_{\mathrm{i}2}(y)+\cdots \tag{25}$$

Equations (16) to (23) in the series form using Eqs. (24) and (25) take the form

Zeroth-order equations ($Br=0$)

Region-I

$$\frac{d^2u_{10}}{\mathrm{d}y^2}-\sigma^2u_{10}=-(1-\phi)^{2.5}\left((1-\phi)+\frac{\phi(\rho\beta)_\mathrm{s}}{(\rho\beta)_\mathrm{f}}\right)Gr\,\theta_{10}-(1-\phi)^{2.5}P \tag{26}$$

$$\frac{d^2\theta_{10}}{\mathrm{d}y^2}=0 \tag{27}$$

Region-II

$$\frac{d^2u_{20}}{\mathrm{d}y^2}=-Gr\ \ \theta_{20}-P \tag{28}$$

$$\frac{d^2\theta_{20}}{\mathrm{d}y^2}=0 \tag{29}$$

Region-III

$$\frac{d^2u_{30}}{\mathrm{d}y^2}-\sigma^2u_{30}=(1-\phi)^{2.5}\left((1-\phi)+\frac{\phi(\rho\beta)_\mathrm{s}}{(\rho\beta)_\mathrm{f}}\right)Gr\,\theta_{30}-(1-\phi)^{2.5}P \tag{30}$$

$$\frac{d^2\theta_{30}}{\mathrm{d}y^2}=0 \tag{31}$$

Zeroth-order boundary and interface conditions become

$$u_{10}(-1)=0,\ u_{10}(0)=u_{20}(0),\ \frac{\mathrm{d}u_{10}(0)}{\mathrm{d}y}=\frac{\mu_\mathrm{f}}{\mu_\mathrm{nf}}\frac{\mathrm{d}u_{20}(0)}{\mathrm{d}y}$$
$$u_{20}(1)=u_{30}(1),\quad \frac{\mathrm{d}u_{20}(1)}{\mathrm{d}y}=\frac{\mu_\mathrm{nf}}{\mu_\mathrm{f}}\frac{\mathrm{d}u_{30}(1)}{\mathrm{d}y},\quad u_{30}(2)=0 \tag{32}$$

$$\theta_{10}(-1)=0,\quad \theta_{10}(0)=\theta_{20}(0),\quad \frac{d\theta_{10}(0)}{\mathrm{d}y}=\frac{k_\mathrm{f}}{k_\mathrm{nf}}\frac{d\theta_{20}(0)}{\mathrm{d}y}$$
$$\theta_{20}(1)=\theta_{30}(1),\quad \frac{d\theta_{20}(1)}{\mathrm{d}y}=\frac{k_\mathrm{nf}}{k_\mathrm{f}}\frac{d\theta_{30}(1)}{\mathrm{d}y},\quad \theta_{30}(2)=1 \tag{33}$$

First-order equations ($Br=1$)

Region-I

$$\frac{d^2u_{11}}{\mathrm{d}y^2}-\sigma^2\,u_{11}=-(1-\phi)^{2.5}\left((1-\phi)+\frac{\phi(\rho\beta)_\mathrm{s}}{(\rho\beta)_\mathrm{f}}\right)Gr\,\theta_{11} \tag{34}$$

$$\frac{d^2\theta_{11}}{\mathrm{d}y^2}=-\frac{1}{(1-\phi)^{2.5}}\left(\frac{2k_\mathrm{f}+\phi(k_\mathrm{f}-k_\mathrm{s})+k_\mathrm{s}}{2k_\mathrm{f}-2\phi(k_\mathrm{f}-k_\mathrm{s})+k_\mathrm{s}}\right)\left(\left(\frac{\mathrm{d}u_{10}}{\mathrm{d}y}\right)^2+\sigma^2u_{10}^2\right)=0 \tag{35}$$

Region-II

$$\frac{d^2u_{21}}{\mathrm{d}y^2}=-Gr\,\theta_{21} \tag{36}$$

$$\frac{d^2\theta_{21}}{\mathrm{d}y^2}=-\left(\frac{\mathrm{d}u_{20}}{\mathrm{d}y}\right)^2 \tag{37}$$

Region-III

$$\frac{d^2u_{31}}{\mathrm{d}y^2}-\sigma^2u_{31}=(1-\phi)^{2.5}\left((1-\phi)+\frac{\phi(\rho\beta)_\mathrm{s}}{(\rho\beta)_\mathrm{f}}\right)\ \ Gr\,\theta_{31} \tag{38}$$

$$\frac{d^2\theta_{31}}{\mathrm{d}y^2}=-\frac{1}{(1-\phi)^{2.5}}\left(\frac{2k_\mathrm{f}+\phi(k_\mathrm{f}-k_\mathrm{s})+k_\mathrm{s}}{2k_\mathrm{f}-2\phi(k_\mathrm{f}-k_\mathrm{s})+k_\mathrm{s}}\right)\left(\left(\frac{\mathrm{d}u_{30}}{\mathrm{d}y}\right)^2+\sigma^2u_{30}^2\right) \tag{39}$$

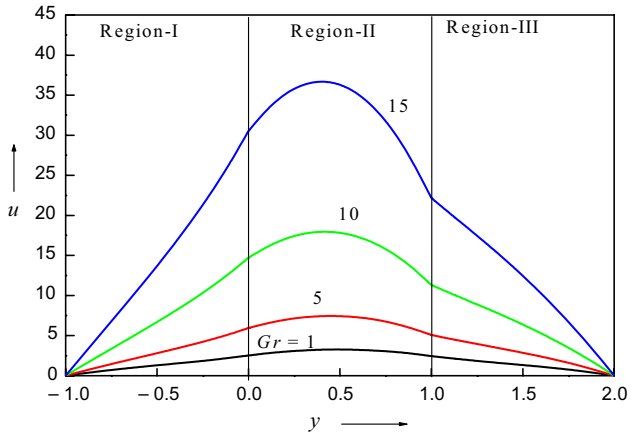

Fig. 2 Velocity profiles for different values of Gr with $Br=0.1$, $\phi=0.02$, $P=5$, $\sigma=2$

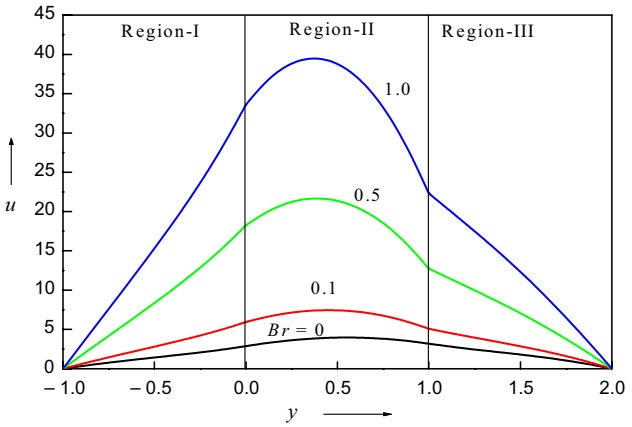

Fig. 3 Temperature profiles for different values of Gr with $Br=0.1$, $\phi=0.02$, $P=5$, $\sigma=2$

First-order boundary and interface conditions become

$$u_{11}(-1)=0,\quad u_{11}(0)=u_{21}(0),\quad \frac{\mathrm{d}u_{11}(0)}{\mathrm{d}y}=\frac{\mu_{\mathrm{f}}}{\mu_{\mathrm{nf}}}\frac{\mathrm{d}u_{21}(0)}{\mathrm{d}y}$$
$$u_{21}(1)=u_{31}(1),\quad \frac{\mathrm{d}u_{21}(1)}{\mathrm{d}y}=\frac{\mu_{\mathrm{nf}}}{\mu_{\mathrm{f}}}\frac{\mathrm{d}u_{31}(1)}{\mathrm{d}y},\quad u_{31}(2)=0 \tag{40}$$

$$\theta_{11}(-1)=0\quad \theta_{11}(0)=\theta_{21}(0),\quad \frac{d\theta_{11}(0)}{\mathrm{d}y}=\frac{k_{\mathrm{f}}}{k_{\mathrm{nf}}}\quad \frac{d\theta_{21}(0)}{\mathrm{d}y}$$
$$\theta_{21}(1)=\theta_{31}(1),\quad \frac{d\theta_{21}(1)}{\mathrm{d}y}=\frac{k_{\mathrm{nf}}}{k_{\mathrm{f}}}\quad \frac{d\theta_{31}(1)}{\mathrm{d}y},\quad \theta_{31}(2)=0 \tag{41}$$

The second-order and higher order terms of the series are neglected. Equations (26)–(41) are ordinary differential equations and therefore the solutions can be defined directly.

The skin friction and Nusselt number in dimensionless form have the following form

$$\tau|_{y=-1}=\frac{\mu_{\mathrm{nf}}}{\mu_{\mathrm{f}}}\left(\frac{\mathrm{d}u_1}{\mathrm{d}y}\right)_{y=-1},\quad \tau|_{y=2}=\frac{\mu_{\mathrm{nf}}}{\mu_{\mathrm{f}}}\left(\frac{\mathrm{d}u_3}{\mathrm{d}y}\right)_{y=2},$$
$$Nu|_{y=-1}=\frac{k_{\mathrm{nf}}}{k_{\mathrm{f}}}\left(\frac{d\theta_1}{\mathrm{d}y}\right)_{y=-1},\quad Nu|_{y=2}=\frac{k_{\mathrm{nf}}}{k_{\mathrm{f}}}\left(\frac{d\theta_3}{\mathrm{d}y}\right)_{y=2}.$$

Results and discussion

Mixed convection in a vertical parallel plate channel with viscous fluid sandwiched between nanofluids saturated within the porous medium is studied analytically. The non-linear differential equations governing the motion have been solved by the perturbation method and exact

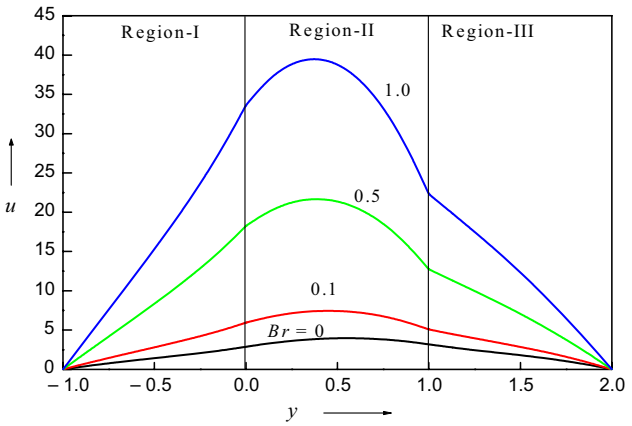

Fig. 4 Velocity profiles for different values of Br with $Gr=5$, $\phi=0.02$, $P=5$, $\sigma=2$

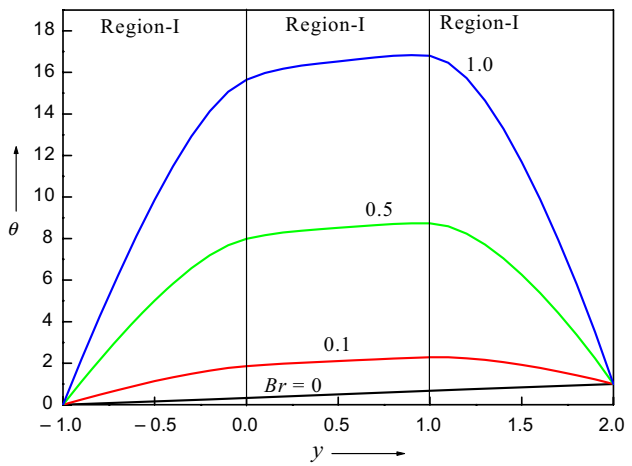

Fig. 5 Temperature profiles for different values of Br with $Gr=5$, $\phi=0.02$, $P=5$, $\sigma=2$

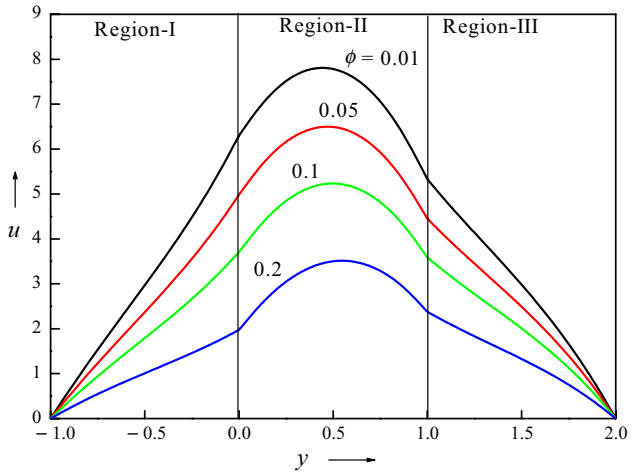

Fig. 6 Velocity profiles for different values of ϕ with $Br=0.1$, $Gr=5$, $P=5$, $\sigma=2$

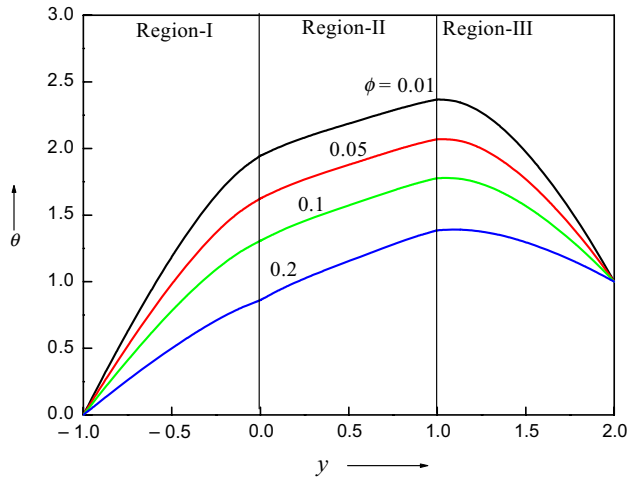

Fig. 7 Temperature profiles for different values of ϕ with $Br=0.1$, $Gr=5$, $P=5$, $\sigma=2$

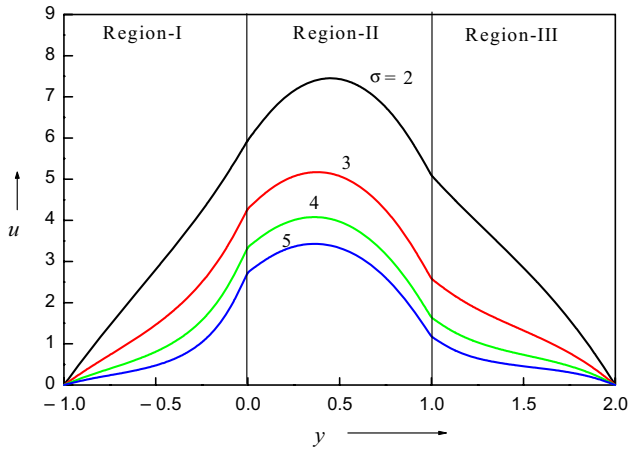

Fig. 8 Velocity profiles for different values of σ with $Gr=5$, $Br=0.1$, $\phi=0.02$, $P=5$

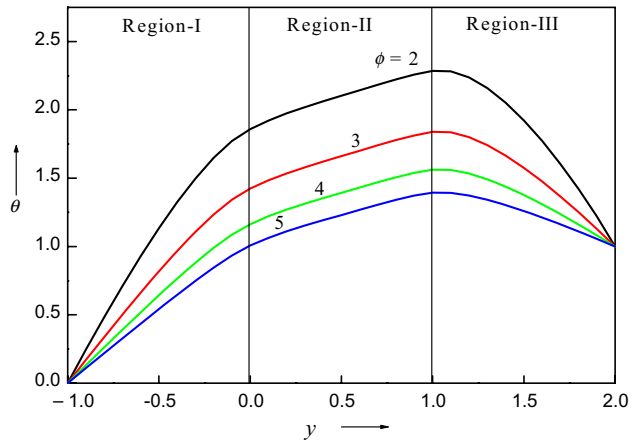

Fig. 9 Temperature profiles for different values of σ with $Gr=5$, $Br=0.1$, $\phi=0.02$, $P=5$

solutions are obtained. The Grashof number Gr, Brinkman number Br, solid volume fraction ϕ, porous parameter σ and the non-dimensional pressure gradient P in all the regions are chosen as 5, 0.01, 0.02, 2 and 5, respectively. The numerical results are presented in Figs. 2–9 that will give a good understanding of the influence of different parameters on velocity and temperature fields.

The velocity variation owing to the growth of the Grashof number Gr is presented in Fig. 2. It is obvious that the velocity is raised with a growth of the Grashof number which characterizes that the flow accelerates as Grashof number increases. It can also be stated from Fig. 2 that the magnitudes of velocity in region-I and region-III are similar, while velocity within region-II is high. In region-I and region-III, the fluid is saturated within the porous medium, and hence the magnitude of velocity is less in comparison with the magnitude of velocity in region-II which is occupied by a clear viscous fluid. The influence of variation of Grashof number on temperature profiles is presented graphically in Fig. 3. It is noticed that as Gr increases the temperature field is also enhanced. Accelerating the Grashof number elevates the thermal buoyancy forces and this helps to escalate the temperatures due to the coupling effect. Though the fluid is saturated within the porous medium in region-I and III and pure viscous fluid is in region-II, but still the magnitude of the temperature in region-III is high in comparison with region-I and region-II. This is due to the heating effect chosen at the boundary. The left plate is at low temperature and it is doubled at the right plate and also for the reasons that the region-II (viscous fluid) also helps to increase the temperature through the dragging of interfacial effects in region-III.

The influence of variation of the Brinkman number on the velocity and temperature fields is presented graphically in Figs. 4 and 5, respectively. The flow and heat transfer in all the regions are enhanced by escalating Brinkman number. The temperature profile in the absence of Brinkman number is linear because the heat is transferred only by conduction. As Brinkman number increases the viscous dissipation is also enhanced which accounts for inclusion of convection through kinetic energy and hence the temperature field is hiked. Due to coupling effect, an increase in temperature accounts for increase in velocity also through the buoyancy terms $Gr\theta_1$, $Gr\theta_2$, $Gr\theta_3$ in region-I, region-II, region-III, respectively. Figure 4 also illustrates that the magnitude of velocity in region-II is large in comparison with region-I and region-III which is the similar observation made in Fig. 2. The reason for this nature is similar justification as explained for Fig. 2. Figure 5 also attains maximum temperature in region-III in comparison with region-I and region-II and the reasoning is explained as above for Fig. 3.

Figures 6 and 7 demonstrate the influence of nanoparticles concentration on the flow and heat transfer. It can be seen that the velocity and temperature fields decrease as the solid volume fraction increases. An increase in solid volume fraction physically implies that nanoparticles concentration becomes high, and hence these suspensions will not allow the base fluid to flow freely. That is to say that the nanofluid becomes dense by increasing the concentration of the nanoparticles which in turn suppresses the flow. Reduction in the velocity results in the reduction of temperature also due to the coupling effect. One should also notice that though fluid in region-II is clear viscous fluid but still solid volume fraction also influence the flow in this region-II. This is again due to the dragging effect of the interfacial conditions as region-I ($\phi \neq 0$) drags the fluid in region-II ($\phi = 0$) and region-III ($\phi \neq 0$) drags the fluid in region-II. The effect of ϕ on the flow is also similar to the results observed by Shekhar and Umavathi [40] and Umavathi et al. [41–43] for the channel filled with only one fluid.

Figures 8 and 9 represent the influence of porous parameter σ on the velocity and temperature fields. The porous parameter σ reduces both the velocity and temperature in all the regions owing to the increased Darcian drag counteracting the flow. The medium permeability decreases substantially with large values of σ and therefore it inhibits the thermal convection. The retardation in the flow is due to the frictional drag resistance. The heat transfer will tend to conduction by decreasing the permeability of the porous medium which cools the fluid in all the three regions. Though the fluid in region-II is not saturated within the porous medium, it is influenced by the nanofluid saturated porous media in region-I and region-III through the interfacial assumptions that the velocities and temperatures are continuous at the two interfaces.

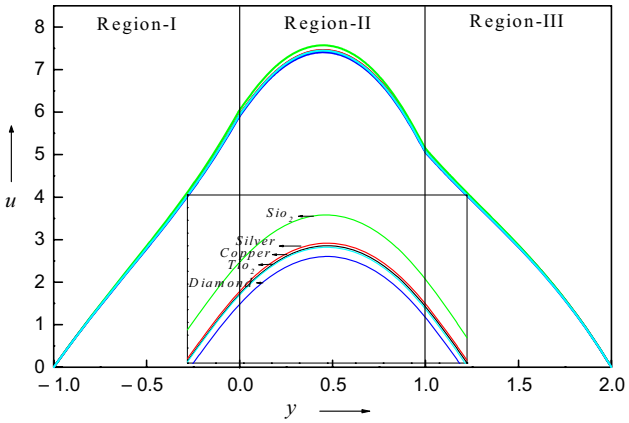

Fig. 10 Velocity profiles for different nanoparticles materials with $Gr=5$, $Br=0.1$, $\phi=0.02$, $P=5$, $\sigma=2$

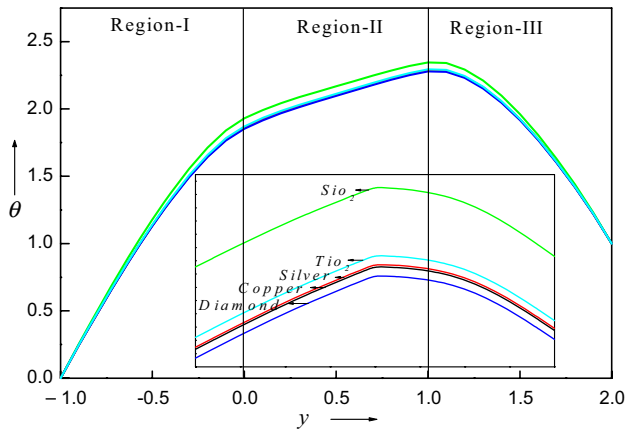

Fig. 11 Temperature profiles for different nanoparticles materials with $Gr=5$, $Br=0.1$, $\phi=0.02$, $P=5$, $\sigma=2$

Using water as the base fluid and copper as the suspended nanoparticles material, the effect of different nanoparticles on the fluid flow is depicted in Figs. 10 and 11. These figures characterize that both the velocity and temperature fields are not distorted by the presence of any of the nanoparticles. By locating a small scale for the y-axis, the profiles are magnified and inform that maximum velocity and temperature can be found for nanoparticles of silicon oxide and minimum values can be found for nanoparticles of diamond.

Table 2 illustrates the numerical values of skin friction and Nusselt number. The Nusselt number graduated at the left border and depleted at the right border for mounting the Brinkman and Grashof numbers. The nanoparticles concentration and the porous parameter decrease the energy transport rate at the left plate and increase it at the right plate. The Nusselt number is optimum at the left plate using silver as the nanoparticles material and minimal value can be obtained using silicon oxide as the

Table 2 Values of Nusselt number and skin friction for $Gr=5$, $Br=0.1$, $\phi=0.02$, $P=5$, $\sigma=2$ except the varying parameter

	$[Nu]_{y=-1}$	$[Nu]_{y=2}$	$[\tau]_{y=-1}$	$[\tau]_{y=2}$
Gr				
1	1.68526	− 1.06152	3.52186	− 3.80517
5	2.68547	− 2.46548	6.6199	− 8.32223
10	4.35022	− 4.91815	14.6007	− 19.5405
Br				
0.01	0.580492	0.0653965	4.03692	− 5.74718
0.1	2.68547	− 2.46548	6.6199	− 8.32223
0.5	12.0409	− 13.7138	18.0998	− 19.7669
ϕ				
0.0	2.7913	− 2.60938	6.99269	− 8.67611
0.02	2.68547	− 2.46548	6.6199	− 8.32223
0.05	2.53432	− 2.25713	6.12136	− 7.86443
σ				
2	2.68547	− 2.46548	6.6199	− 8.32223
6	1.03376	− 0.362388	1.03133	− 1.74456
10	0.766965	0.231202	0.537141	− 1.0053
Cu	2.68547	− 2.46548	6.6199	− 8.32223
Ag	2.68752	− 2.46947	6.63055	− 8.3449
SiO_2	2.67103	− 2.45617	6.71506	− 8.36831
Diamond	2.67735	− 2.44959	6.57678	− 8.23142
TiO_2	2.67554	− 2.45068	6.60854	− 8.2612

nanoparticles material. At the right plate, the optimum energy transport intensity is obtained using the silver nanoparticles and minimum value is obtained using titanium oxide as the nanoparticles material. However, there is no significant change in the thermal transmission intensity using different types of nanoparticles material.

The skin friction increases at the left wall for increasing in the values of Grashof number and Brinkman number, whereas it declines at the right wall. The effects of solid volume fraction and porous parameter are to decrease the skin friction at the left border and increase at the right border. The optimal skin friction value is obtained using the silicon oxide as nanoparticles material at both the left and right plates, whereas the minimal value is obtained using titanium oxide as the nanoparticles material.

The considered results are compared with data presented by Vajravelu et al. [44]. The coefficients of the present problem and from the data of Vajravelu et al. [44] are matched as follows. The values used for the comparison are $Gr=\lambda=5$, $Ec\cdot Pr=Br=0.01$, $a_1b_1=m_1c_1\beta_1/\beta_2=a$ and $1/(a_1d_1)=\alpha_1/(m_1c_1\alpha_2)=b$, where $b_1=\beta_2/\beta_1$, $a_1=m_1C_1, C_1=\rho_2/\rho_1, d_1=\alpha_2/\alpha_1$ α_1 and α_2 are thermal diffusivity of region-I and region-II, respectively, $a=(1-\phi)^{2.5}\left((1-\phi)+\phi\frac{(\rho\beta)_s}{(\rho\beta)_f}\right)$, $b=\frac{1}{(1-\phi)^{2.5}}\left(\frac{2k_f+\phi(k_f-k_s)+k_s}{2k_f-2\phi(k_f-k_s)+k_s}\right)$ and $\phi=0.02$. It is seen that the present magnitude and the values obtained by Vajravelu et al. [40] are found to be equal.

Conclusions

The problem of mixed convection of a viscous fluid sandwiched between saturated nanofluid zones through vertical parallel plates under the impact of a fixed pressure gradient was investigated. The analytical solutions were defined using the perturbation method for the velocity and temperature fields within three different zones. The physical parameters describing the flow as well as energy transport intensity and skin friction at the left and right borders of the channels were also analyzed for different parametric conditions. It was revealed that

1. Brinkman number and Grashof number escalate the velocity and temperature fields, where as the solid volume fraction and porous parameter suppress the flow.
2. More intensive flow was seen for silicon oxide as the nanoparticle material, while the lowest flow was observed using diamond as the nanoparticles material keeping water as the base fluid. However, there was no distinguishable influence on the flow using any nanoparticles material.
3. Enhancing Brinkman and Grashof numbers, the Nusselt number elevates at the left wall and shrinks at the right wall. The nanoparticles concentration and the porous parameter reduce the thermal transmission intensity at the left border and expand it at the right wall. The Nusselt number has highest values at the left wall using silver as the nanoparticles material and the modest values are obtained using the silicon oxide as the nanoparticles material. At the right wall, the classical heat transfer rate in magnitude is obtained using silver as the nanoparticles material and the lowest is obtained using titanium oxide as the nanoparticles material. However, there is no significant change in the rate of heat transfer using different types of nanoparticles.
4. The skin friction increases at the left plate for increasing the values of Grashof number and Brinkman number whereas it shrinks at the right wall. The effect of solid volume fraction and porous parameter lessens the skin friction at the left wall and expands at the right wall. The optimal skin friction in magnitude is obtained using silicon oxide as the nanoparticle at both the left and right plate whereas the minutest is obtained for titanium oxide as the nanoparticle.

Acknowledgements This work of Mikhail A. Sheremet was supported by the Regional Scientific and Educational Mathematical Centre of Tomsk State University.

References

1. Maxwell JA. Treatise on electricity and magnetism. 2nd ed. Oxford: Clarendon Press; 1873.
2. Selimefendigil F, Chamkha AJ. Magnetohydrodynamics mixed convection in a power law nanofluid-filled triangular cavity with an opening using Tiwari and Das' nanofluid model. J Therm Anal Calorim. 2019;135:419–36.
3. Izadi M, Hashemi Pour SMR, Yasuri AK, Chamkha AJ. Mixed convection of a nanofluid in a three-dimensional channel. Effect of opposed buoyancy force on hydrodynamic parameters, thermal parameters and entropy generation. J Therm Anal Calorim. 2019;136:2461–75.
4. Ahmed SE, Mansour MA, Hussein AK, Mallikarjuna B, Almeshaal MA, Kolsi L. MHD mixed convection in an inclined cavity containing adiabatic obstacle and filled with Cu–water nanofluid in the presence of the heat generation and partial slip. J Therm Anal Calorim. 2019;138:1443–600.
5. Bondarenko DS, Sheremet MA, Oztop HF, Abu-Hamdeh N. Mixed convection heat transfer of a nanofluid in a lid-driven enclosure with two adherent porous blocks. J Therm Anal Calorim. 2019;135:1095–105.
6. Abu-Nada E, Chamkha AJ. Mixed convection flow in a lid-driven inclined square enclosure filled with a nanofluid. Eur J Mech B Fluids. 2010;29:472–82.
7. Tiwari RK, Das MK. Heat transfer augmentation in a two sided lid-driven differentially heated square cavity utilizing nanofluids. Int J Heat Mass Transf. 2007;50:2002–188.
8. Mittal N, Satheesh A, Kumar DS. Numerical simulation of mixed-convection flow in a lid-driven porous cavity using different nanofluids. Heat Transf Asian Res. 2014;43:1–16.
9. Bianco V, Manca O, Nardini S, Vafai K. Heat transfer enhancement with nanofluids. New York: CRC Press; 2015.
10. Bianco V, Manca O, Nardini S. Second law analysis of Al_2O_3-water nanofluid turbulent forced convection in a circular cross section tube with constant wall temperature. Adv Mech Eng. 2013;5:1–12.
11. Bianco V, Manca O, Nardini S. Performance analysis of turbulent convection heat transfer of Al_2O_3 water-nanofluid in circular tubes at constant wall temperature. Energy. 2014;77:403–13.
12. Lee S, Choi SUS, Li S, Eastman JA. Measuring thermal conductivity of fluids containing oxide nanoparticles. J Heat Transf. 1999;121:280–9.
13. Mostafizur RM, Saidur R, Abdul Aziz AR, Bhuiyan MHU. Thermo physical properties of methanol based Al_2O_3 nanofluids. Int J Heat Mass Transf. 2015;85:414–9.
14. Choi SUS, Zhang ZG, Lockwood FE, Grulke EA. Anomalous thermal conductivity enhancement in nanotube suspensions. Appl Phys Lett. 2001;79:2252–4.
15. Ellahi R, Hassan M, Zeeshan A. Shape effects of nanosize particles in Cu-H_2O nanofluid on entropy generation. Int J Heat Mass Transf. 2015;81:449–56.
16. Sheikholeslami M, Ellahi R, Hassan M, Soleimani S. A study of natural convection heat transfer in a nanofluid filled enclosure with elliptic inner cylinder. Int. J. Numer Methods Heat Fluid Flow. 2014;24:1906–27.
17. Sheikholeslami M, Ellahi R, Ashorynejad HR, Domairry G, Hayat T. Effects of heat transfer in flow of nanofluids over a permeable stretching wall in a porous medium. J Comput Theor Nanosci. 2014;11:486–96.
18. Akbar NS, Raza M, Ellahi R. Interaction of nanoparticles for the peristaltic flow in an asymmetric channel with the induced magnetic field. Eur Phys J Plus. 2014;129:155–67.
19. Akbar NS, Raza M, Ellahi R. Influence of heat generation and heat flux on peristaltic low with interacting nanoparticles. Eur Phys. 2014;129:185–99.
20. Sheikholeslami M, Bandpy MG, Ellahi R, Zeeshan A. Simulation of MHD CuO-water nanofluid flow and convective heat transfer considering Lorentz forces. J Magn Magn Mater. 2014;369:69–80.
21. Ding YL, Alias H, Wen DS, Williams RA. Heat transfer of aqueous suspensions of carbon nanotubes (CNT nanofluids). Int J Heat Mass Transf. 2006;49:240–50.
22. Bianco V, Manca O, Nardini S. Numerical simulation of water/Al_2O_3 nanofluid turbulent convection. Adv Mech Eng. 2010;2010:1–10.
23. Sheikholeslami M, Shehzad SA, Li Z, Ahmad S. Numerical modeling for alumina nanofluid magnetohydrodynamic convective heat transfer in a permeable medium using Darcy law. Int J Heat Mass Transf. 2018;127:614–22.
24. Sheikholeslami M, Shehzad SA, Li Z, Ahmad S. Lorentz forces effect on NEPCM heat transfer during solidification in a porous energy storage system. Int J Heat Mass Transf. 2018;127:665–74.
25. Shenoy A, Sheremet M, Pop I. Convective flow and heat transfer from wavy surfaces: viscous fluids, porous media and nanofluids. Boca Raton: CRC Press; 2016.
26. Nield DA, Kuznetsov AV. The Cheng-Minkowycz problem for the double-diffusive natural convective boundary layer flow in a porous medium saturated with a nanofluid. Int J Heat Mass Transf. 2011;54:374–8.
27. Cheng P, Minkowycz W. Free convection about a vertical flat plate embedded in a porous medium with application to heat transfer from a dike. J Geophysical Research. 1977;82:2040–4.
28. Umavathi JC, Mohite MB. The onset of convection in a nanofluid saturated porous layer using Darcy model with cross diffusion. Meccanica. 2014;49:1159–75.
29. Ahmed S, Pop I. Mixed convection boundary layer flow from a vertical flat plate embedded in a porous medium filled with nanofluids. Int Commun Heat Mass Transf. 2010;37:987–91.
30. Sheikholeslami M. Magnetic field influence on CuO-H_2O nanofluid convective flow in a permeable cavity considering various shapes for nanoparticles. Int J Hydrogen Energy. 2017;42:19611–21.
31. Cimpean D, Pop I. Fully developed mixed convection flow of a nanofluid through an inclined channel filled with a porous medium. Int J Heat Mass Transf. 2012;55:907–14.
32. Hajipour M, Dehkordi A. Analysis of nanofluid heat transfer in parallel-plate vertical channel filled with porous medium. Int J Therm Sci. 2012;55:103–13.
33. Amrei Hashemi SMH, Dehkordi AM. Modeling and CFD simulation of a mixed-convection flow of regular fluids and nanofluids in vertical porous and regular channels. Heat Transf Asian Res. 2014;43:243–69.
34. Hatami M, Sheikholeslami M, Ganji DD. Nanofluid flow and heat transfer in an asymmetric porous channel with expanding or contracting wall. J Mol Liq. 2014;195:230–9.
35. Sheikholeslami M, Kataria HR, Mittal AS. Effect of thermal diffusion and heat-generation on MHD nanofluid flow past an oscillating vertical plate through porous medium. J Mol Liq. 2018;257:12–25.
36. Hajizadeh A, Shah NA, Shah SIA, Animasaun IL, Rahimi-Gorji M, Alarifi IM. Free convection flow of nanofluids between two vertical plates with damped thermal flux. J Mol Liq. 2019;289:110964.

37. Sheikholeslami M. Numerical approach for MHD Al_2O_3-water nanofluid transportation inside a permeable medium using innovative computer method. Comput Methods Appl Mech Eng. 2019;344:306–18.
38. Vafai K, Thiyagaraja R. Analysis of flow and heat transfer at the interface region of a porous medium. Int J Heat Mass Transf. 1987;30:1391–405.
39. Brinkman HC. The viscosity of concentrated suspensions and solutions. J Chem Phys. 1952;20:571–81.
40. Shekhar M, Umavathi JC. Influence of viscous dissipation on non-Darcy mixed convection flow of nanofluid. Heat Transf Asian Res. 2017;46:176–99.
41. Umavathi JC, Liu IC, Sheremet MA. Convective heat transfer in a vertical rectangular duct filled with nanofluid. Heat Transf Asian Res. 2016;45:661–79.
42. Umavathi JC, Sheremet MA. Influence of temperature dependent conductivity of a nanofluid in a vertical rectangular duct. Int J Non-Linear Mech. 2016;78:17–28.
43. Umavathi JC, Ojjela O, Vajravelu K. Numerical analysis of natural convective flow and heat transfer of nanofluids in a vertical rectangular duct using Darcy–Forchheimer–Brinkman model. Int J Therm Sci. 2017;111:511–24.
44. Vajravelu K, Prasad KV, Abbasandy S. Convective transport of nanoparticles in multi-layer fluid flow. Appl Math Mech Engl Ed. 2013;34:177–88.